PERGAMON International Journal of Multiphase Flow 24 (1998) 1295–1315

International Journal of Multiphase Flow

# Monofiber optical probes for gas detection and gas velocity measurements: optimised sensing tips

A. Cartellier *, E. Barrau

*LEGI, Laboratoire des Écoulements Géophysiques et Industriels, UMR 5519 UJF-CNRS-INPG, BP 53, F-38041, Grenoble cedex 9, France*

Received 28 November 1996; received in revised form 11 March 1998

**Abstract**

In order to perform gas velocity measurements using a single optical probe, an optimisation of the probe geometry has been undertaken. The responses of conical probes, analysed in a previous article, were found to be strongly sensitive to deviations from an ideal geometry. To render the technique much sounder, two new shapes, namely, cone + cylinder (2C) and cone + cylinder + cone (3C) are considered. They are both effective for simultaneous gas detection and gas velocity measurements, but the latter, free of proximity detection, appears to be the most promising due to a calibration curve, i.e. the relationship between signal rise time and interface velocity, weakly sensitive to uncontrollable parameters such as the interface impact angle. In addition, its latency length can be controlled during the manufacturing process, allowing good reproducibility of probe tips. Analysis of the signal transients is used to provide guidelines for effective signal processing. Finally, possible extensions of the monofiber technique are discussed as well as remaining limitations. © 1998 Elsevier Science Ltd. All rights reserved.

*Keywords:* Optical probe; Interface detection; Gas velocity; Interface piercing; Drainage; Bubble size distribution; Interfacial area density; Gas–liquid (flow)

## 1. Introduction

Monofiber optical probes are able to provide the gas velocity provided that their latency length is known (Cartellier, 1992). In order to optimise this technique, conical probes have been studied using a simplified optical simulation and well-controlled piercing experiments performed on actual probes (Cartellier and Barrau, 1998; hereafter referred to as part I).

* Corresponding author.


PII: S0301-9322(98)00033-0

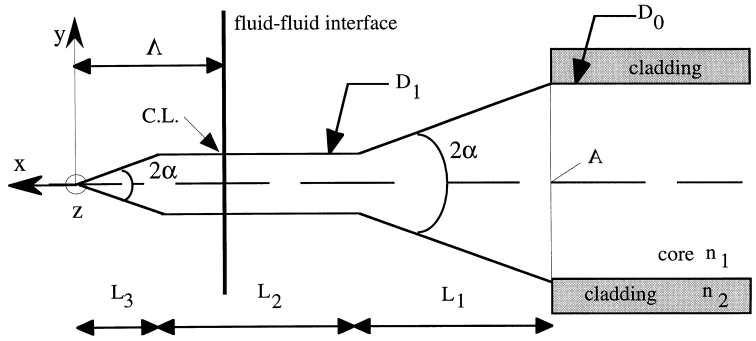


Fig. 1. Geometrical parameters defining the idealised fiber tips.

Although a perfect cone was recognised as potentially a well-suited geometry, this shape appears quite sensitive to imperfections, especially if located at the tip. Indeed, cleaved cones produce pre-signals which can induce erroneous phase detection. Beside, their latency lengths are strongly altered by the presence of such defects. In order to better control the probe performance through the manufacturing process, new shapes are considered. Since the addition of a cylindrical section to the sensing tip is expected to bring some benefit, geometries such as conical + cylindrical (hereafter referred as 2C) and conical + cylindrical + conical (hereafter referred as 3C) schematised in Fig. 1, are now investigated. Such shapes can be produced using the manufacturing technique described in part I: examples are presented in Fig. 2. The responses of such prototypes during well-controlled transitions through liquid–gas interfaces

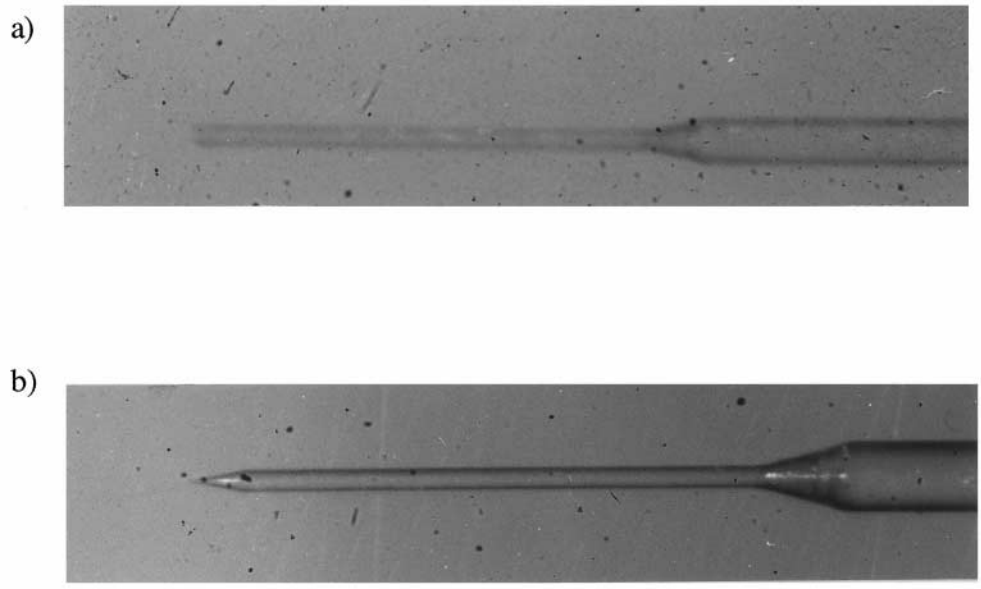


Fig. 2. Examples of probe tips produced by the etching technique (the fiber external diameter at the right hand side is 140 $\mu$m).

are tested and compared with predictions in Sections 2 and 3. Their ability to obtain the gas phase velocity in actual two-phase flow is analysed in connection with the signal processing sequence in Sections 4 and 5.

## 2. Cone + cylinder probes (2C)

### 2.1. Simulation of 2C probes

This geometry is defined by three free parameters: the half cone angle $\alpha$, the diameter $D_1$ and the length $L_2$ of the cylindrical portion, while $L_1$ is given by $[D_0\text{-}D_1]/[2 \tan \alpha]$ (Fig. 1). The optical simulation presented in part I is used again: it provides an estimate of the signal amplitude for wet and dry probes as well as the evolution of the reflection coefficient $R$ for a planar interface sliding along the probe tip. The optical fiber considered has a core index of 1.46, a cladding index of 1.44 (N.A. = 0.24) and a core diameter $D_0$ of 100 $\mu$m. The external media are air and water.

Let us first consider the phase discrimination property of 2C probes. The reflection coefficients of 2C probes evolve with $D_1$ and $\alpha$ in a similar manner to those of cleaved conical tips. Indeed, the same three populations of rays, as shown in Fig. 3, intervene in the process:

- population 1—consisting of rays directly impacting the flat end;
- population 2—formed by rays subject to the reversing process due to reflections on the cone sides and which do not touch the flat extremity;
- population 3—corresponding to rays impacting the flat end after some deviation by the cone sides.

The first and second populations (rays directly impacting the flat end and reversed by the cone, respectively) behave as discussed in part I, Section 4-A, for a cleaved conical tip. The presence of a cylindrical portion introduces additional constraints on the ray path for the third population, which now corresponds to rays deflected by the conical sides before entering the cylinder. Again, discarding the limiting cases $D_1 \rightarrow 0$ and $D_1 \rightarrow D_0$, this third population is the most active and is responsible for the probe response. Let us investigate its behaviour. The cylinder acts as a wave guide according to the external medium and ray inclination. Denoting

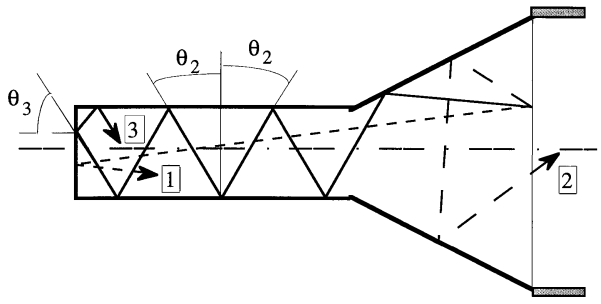


Fig. 3. The three populations of active rays for a 2C geometry.

$N$ as the number of impacts on the cone during forward propagation, the incidence angle $\theta_2$ on the surface of the cylinder is given by $\pi/2-2N\alpha\text{-}\theta_0$. Total guidance is ensured when $\theta_2$ exceeds the critical angle $\theta_c$ at the fiber core/external medium boundary. Rays with an incidence of less than $\theta_c$ are only partially reflected upon meeting the boundary, and since $\theta_2$ remains the same along the cylinder, attenuation increases with $L_2$. At the flat tip, the incidence $\theta_3$ equals $\pi/2-2N\alpha\text{-}\theta_2$, and total reflection occurs when $\theta_3$ exceeds $\theta_c$. Then the ray returns back along the cylinder with the same incidence $\theta_2$. The collection condition by the unaltered fiber applies after one or more reflections on the cone sides. However, to understand how a 2C geometry reacts to phase change, it is sufficient to investigate the conditions for guidance in the cylinder, and the reflection at the tip, since they will provide the most powerful contributions to the signal. Other constraints due to the precise geometry, partial reflections and fiber numerical aperture N.A. have a second-order influence. Thus, a high signal is associated with the conditions: $\theta_2 > \theta_c$ and $\pi/2- \theta_2 > \theta_c$. To qualitatively understand the behaviour of such rays, the angle $\theta_2$ is plotted vs the half tip angle $\alpha$ in Fig. 4 for various integer values of $N$. Due to the angular range available at injection, each line at $N$ constant should be thought as a band of width 2 $\Theta_m$. On the ordinate scale, the critical angles and their complement to $\pi/2$ are plotted both for core/water and core/air boundaries. The above inequalities concerning total reflection at the flat extremity (T.R.) and total guidance in the cylinder (T.G.) conditions are represented by intervals in Fig. 4. To interpret this figure, let us fix a value of $\alpha$, say 14°. The intersections between the vertical line $\alpha$ = constant and the lines $N$ = constant provide the rays penetrating the cylinder. At $\alpha = 14°$, four rays are active, namely $N = 0$ which belongs to the first population, and $N = 1$–3 which belong to the second one. These solutions are the same for water and for air, and phase discrimination is ensured thanks to the variation of the reflection coefficients.

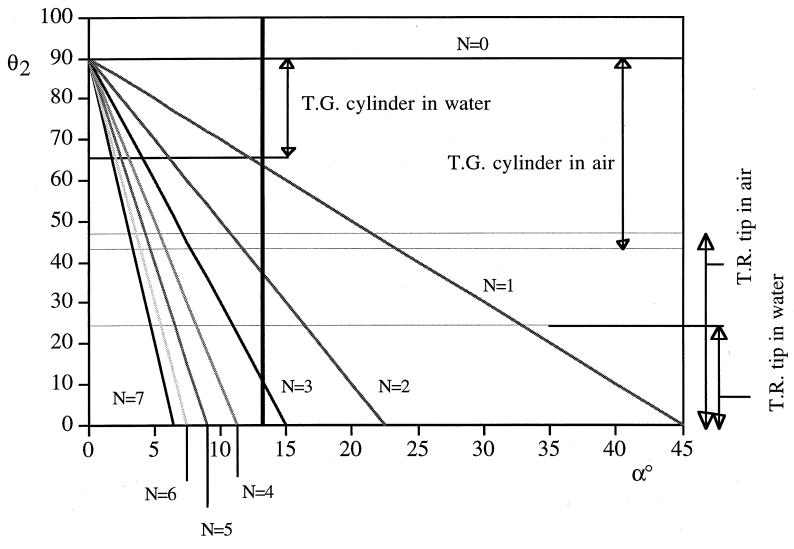


Fig. 4. Determination of active rays for a 2C geometry.

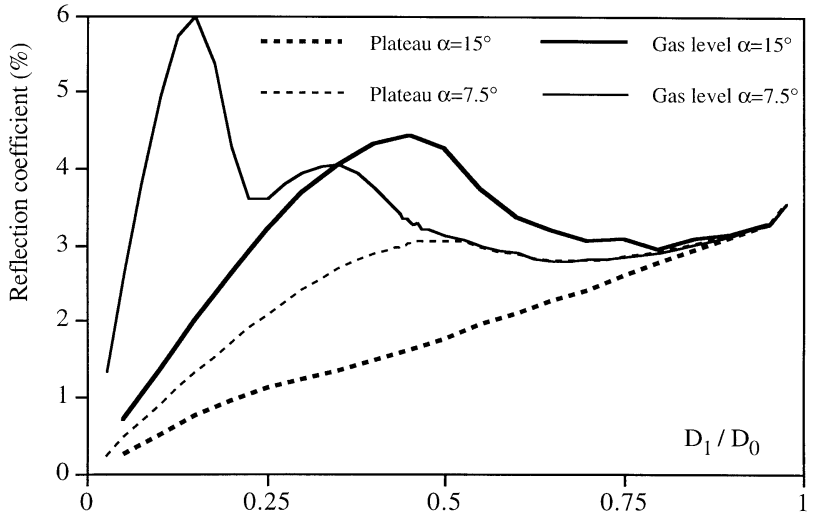


Fig. 5. Evolution of gas and plateau levels with $D_1/D_0$ for 2C probes ($\alpha = 15°$ and 7.5°).

When completely wet, the only active rays totally guided in the cylinder are those directly impacting the flat end, i.e. $N = 0$. For $N = 1$, the reflection coefficient $R'$ at each impact on the cylinder boundary is about 10% and it is even lower as $N$ increases. Moreover, at the flat tip, $R'$ is weak except for $N = 3$, but, in that case, the rays have already been highly attenuated during their propagation in the cylinder. Thus, the amplitude for a wet probe is essentially due to the family of rays $N = 0$ whose contribution is 3.5% to be weighted by their relative number.

For a completely dry probe, the solutions corresponding to $N = 0$ and 1 are fully guided, while $N = 2$ is weakly attenuated because its incidence $\theta_2$ is close to $\theta_c$. Moreover, the solutions for $N = 2$–3 are subject to total reflection at the flat end. Summing these contributions led to a high amplitude, notably because some rays of the family $N = 2$ keep their energy while travelling in and out of the cylinder.

Thus, 2C probes are able to discriminate well between water and air whatever the choice of $\alpha$ and $D_1$. This is confirmed by the simulation and an example of the evolution of $R$ with $D_1$ is given in Fig. 5. The limiting cases $D_1 \rightarrow 0$ and $D_1 \rightarrow D_0$ can be explained by the considerations put forth for cleaved cones (see part I), and again, optimum behaviour exists at a small value of $D_1$. Comparing Figs. 5 and 15 of part I, it is seen that the reflection coefficient at a given tip angle is smaller with the 2C probe than the cleaved cone. This is a consequence of the smaller number of active rays in a 2C geometry compared to cleaved cones due to the limitations imposed by the guidance condition inside the cylinder.

Phase sensitivity is not the only parameter of interest for these 2C geometries. Before discussing this new aspect, it is necessary to examine the transients predicted for 2C probes. Some examples of the response during water exit are given in Fig. 6, where $\alpha$ and $D_1$ are held fixed and $L_2$ is varied. Provided that the cylinder is long enough, the responses consist of three distinct parts:

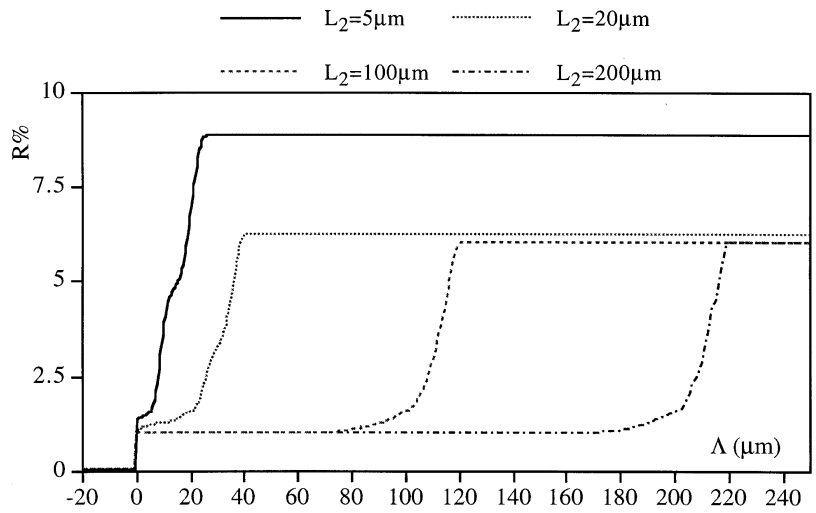


Fig. 6. Predicted transients for 2C probes with various cylinder lengths $L_2$ during water exit ($\alpha = 14°$, $D_1 = 15\ \mu$m).

- A sudden surge due to the drying of the flat extremity, which is instantaneous since the interface is assumed to be planar.
- An intermediate plateau at a constant average reflection coefficient corresponding to the interface sliding along the cylindrical portion while the base cone remains wetted. The plateau length is proportional to the cylinder length $L_2$.
- A smooth increase up to the gas level, the nature of which is dependent upon $D_1$ and $\alpha$. In Fig. 6, this transition region is about 50 $\mu$m.

To these events, one must add a proximity detection prior to the initial surge. Discarding this aspect (not represented in Fig. 6, see part I, Section 3), the interval between the beginning of the signal rise and its end clearly defines the transit time of the interface along the cylinder, and the connection between the latency length and the geometry is now straightforward. The situation is, however, not so ideal when length $L_2$ becomes small, since the plateau and the ramp merge and are difficult to separate. Also, the gas level becomes slightly sensitive to the cylinder length. For example, at $\alpha = 4.8°$, $D_1 = 15\ \mu$m, there is no clear separation between the cylinder and the cone contributions for $L_2$ less than 20 $\mu$m. It should be mentioned that for 2C geometries, the amplitude of the plateau is extremely sensitive to the value of the numerical aperture. A lower N.A. favours the contribution of the flat part vs that of the base cone so that the intermediate plateau increases as N.A. decreases.

An important contribution of this simulation is the prediction of a plateau at a fixed level indicating that the unclad cylindrical part is neutral with respect to signal dynamics. This is not an obvious result since some light is expected to escape to the outer medium, a phenomenon sometimes used in optical sensors (Bobb et al., 1988) for index measurements. To explain this specific response, let us go back to the sketch of Fig. 4, and instead of fully dry or fully wet tips, let us consider an interface located at the boundary between the cone and cylinder (i.e. for $\Lambda = L_2$).

For a base cone surrounded by water, the active rays subject to some reflections along the cone carry a given amount of energy (say $Q$) when they enter the cylinder. They are then subject to the response of the cleaved cylinder which, when surrounded by air, allows a large portion (say $S$) of the incoming energy to come back. When the cone dries, these active rays bring more energy because the partial reflection coefficient on the cone is higher. Thus, the energy entering the cylinder is now $Q'$ with $Q' > Q$, while the fraction that returns back in the fiber due to the cleaved cylinder is the same ($S$). The resulting signal $Q'S$ for a fully dry probe is then higher than the signal $QS$ collected with a dry cylinder and wet cone. It appears that the responses during transients are not composed of a contribution from the cylinder plus another from the cone. The latter has a very weak contribution by itself since it reduces to that of population 2. Instead, the base cone acts as a switch, on in air, off in water, letting more or less energy into the cylinder, and the returning rays (and thus the signal) are always controlled by the response of the cylinder and its tip. The cylinder itself intervenes in the choice of active rays among the possible solutions. If the cylinder is long enough, only totally guided rays are eligible, so that no attenuation occurs along $L_2$, and the signal remains at a constant amplitude $QS$ when the interface slides along the cylinder. Weakly guided active rays can also contribute to the signal and in this case, the amplitude should vary with the interface position along the cylinder. However, the latter contributions are more effective for small cylinder lengths because of the lower number of reflections. Both these tendencies appear in the results of Fig. 6 where the influence of $L_2$ becomes clear below 20 $\mu$m. Finally, depending on its dry or wetted state, the flat end acts as a switch controlling the return of active rays. Thus, 2C probes react as the combined on/off responses of the flat tip and base cone.

In the prospect of velocity measurements, and thus of automatic signal processing adapted to rise time determination, it is desirable not to miss some part of the intermediate plateau because of incorrect thresholding. Thus, it is worthwhile to optimise the choice of parameters $\alpha$ and $D_1$ to ensure a plateau level not too close to liquid and gas levels. As can be seen in Fig. 4, the number of active rays belonging to the third population increases as the half tip angle diminishes, so that the plateau level should increase as $\alpha$ decreases for a fixed diameter $D_1$. At a fixed angle, it is necessary to avoid limiting cases $D_1 \rightarrow 0$ for which the perfect cone is recovered, and $D_1 \rightarrow D_0$ for which the cleaved case is obtained. All these trends are confirmed by Fig. 5, which shows the evolution of the plateau level with $D_1$ for $\alpha = 14^\circ$ and $7.5^\circ$. Thus, there exists an optimal geometry ensuring the presence of a plateau at a level roughly located midway between the water and gas levels. Thanks to a systematic study of these variations, optimum 2C geometries have been defined before being manufactured. For example, at $\alpha = 15^\circ$, a cylinder diameter about 50 $\mu$m should provide a plateau located at 40% of the fully dry probe signal output (provided that $L_2$ is long enough).

Another consequence of the simplified explanation of the 2C probe performance can be set forth by now considering gas-to-liquid transitions. Just after the contact with the interface, the cone is in air, and the amount of energy injected in the cylinder equal to $Q'$ is high. However, once wetted, the critical angle on the tip becomes such that the most powerful active rays ($N = 2$ for $\alpha = 14^\circ$ in Fig. 4) experience a partial reflection, poorly efficient in terms of energy. The efficiency of the cylinder becomes $S'$ instead of $S$, with $S' < S$, and the signal reaches an amplitude $Q'S'$. When both the cylinder and the cone are wetted, the signal drops again down to the level $QS'$. These trends are well recovered on simulations as exemplified in Fig. 7 for a

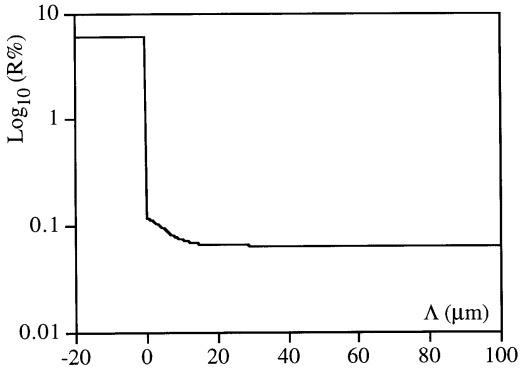


Fig. 7. Predicted transient for 2C probe during water entry ($\alpha = 14°$, $D_1 = 15\ \mu m$, $L_2 = 50\ \mu m$).

particular geometry, except that the signal drop corresponding to the cone rewetting is not seen in this figure because it is less than 1% of the signal amplitude. Let us note that for a gas-to-water transition, the signal drop is $Q'(S–S')$ while its increase for a water-to-gas transition is $Q(S\text{-}S')$. Since $Q' > Q$, the amplitude $Q'S'$ of the plateau observed for gas-to-liquid transition is less than the intermediate plateau level $QS$ observed during the liquid-to-gas transition. Thus, the signal delivered by a 2C probe while crossing a gas inclusion can be schematised as shown in Fig. 8. Note that, although a plateau does exist for gas-to-liquid transitions, its low level does not disturb the detection of the end of the bubble. However, this rear plateau could be annoying for the detection of the beginning of the next bubble because the reference water level is lost. This problem is expected to occur only at high gas concentration, for which the liquid bridges between bubbles are smaller than the latency length of the probe.

### 2.2. Experiments

Quasi-steady piercing experiments have been performed with probe 2C05, shown in Fig. 2a, which has the following characteristics: $L_1 = 140\ \mu m$, $L_2 = 1340\ \mu m$, $D_1 = 58\ \mu m$ and $\alpha \approx 16°$. Liquid-to-gas and gas-to-liquid transitions are presented in Figs. 9 and 10, respectively, for normal impacts. As expected, this prototype is subject to strong proximity detection because of the cleaved tip. Discarding proximity detection, the transitions assume the expected shapes. Indeed, for the water exit configuration, the intermediate plateau is present and has a fairly constant level. Also, the water entry response is abrupt and, at the base of the signal drop, the signal decreases slightly towards the liquid level. The plateau amplitudes are much different

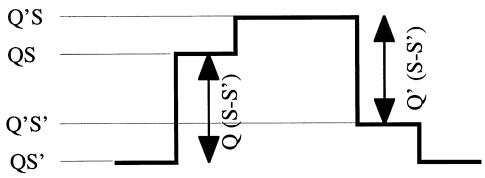


Fig. 8. Schematized response of a 2C probe crossing a gas inclusion.

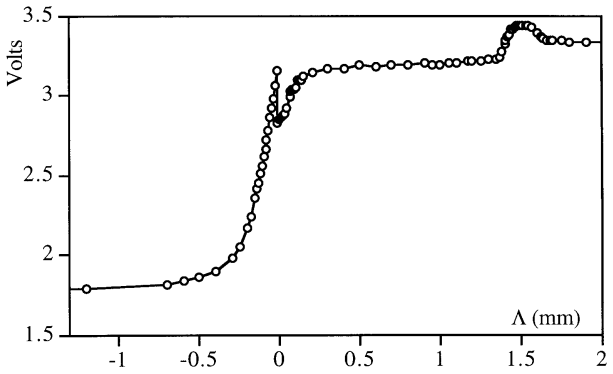


Fig. 9. Quasi-steady response of probe 2C05 during water exit.

from computed values: for the water exit, the recorded level equals 90% of the maximum signal amplitude instead of the 58% predicted by the simulation (recall that the numerical aperture strongly modifies the plateau level). Such discrepancies have no effect on the spatial extent of the transitions since the correct magnitude is recovered for the transition length.

The dynamic response of the 2C05 probe has been investigated on isolated slugs under normal impacts. Some typical signals are presented in Fig. 11 where strong pre-signals can be noticed. Their shapes are quite similar to those observed under quasi-steady conditions except for the relative height of the plateau. As confirmed by all the dynamic piercing experiments on controlled interfaces, the plateau level decreases as the velocity increases: its relative amplitude is about 41% at 0.12 m/s and about 25% at 1.7 m/s. This effect is probably induced by the presence of a liquid film of thickness varying with the velocity (see Section IIB, part I). Again, these levels differ from the predicted value.

The evolution of the latency length with the interface velocity is shown in Fig. 12, where it is scaled either by the length $L_2$ of the cylindrical portion, or by the total length $L_1 + L_2$ of the probe. When specific thresholds for plateau detection are set, the edges of the plateau may be mistakenly identified if proximity detection signals exceed the upper threshold. This indeed occurs at low velocities (below 0.3 m/s) for the 2C05 probe, leading to latency lengths three times lower than expected. Avoiding proximity detection is thus preferable, to ensure physical

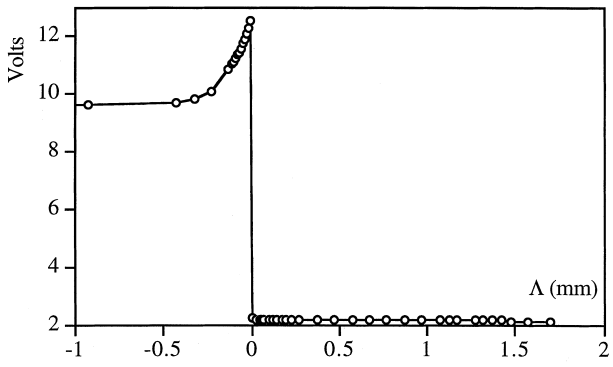


Fig. 10. Quasi-steady response of probe 3C05 during water entry.

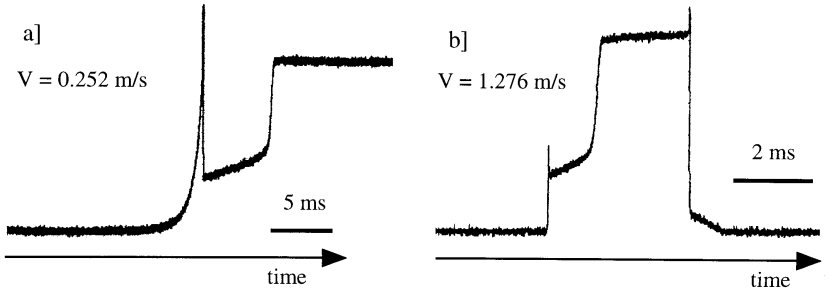


Fig. 11. Water-to-air transitions for probe 2C05 (in trace b, the probe has travelled through a slug and the gas-to-water transition is also visible).

meaning in the measurement. Thus, the latency length has been defined here between the minima following the proximity detection, an event which corresponds to the position of the undisturbed interface, and the 90% level: it is noted $L'$. Clearly, such a latency length is very close to the total sensor length: all values of $L'/(L_1 + L_2)$ are equal to unity within $\pm 5\%$. Compared to the length of the cylindrical portion alone, the latency length $L'$ is 10% higher: this difference represents the contribution of the rear cone to the transition. Thus the experiments confirm the simulation with respect to the shape and the duration of the transitions. The main differences are found for the plateau level whose amplitude cannot be accurately predicted without introducing the hydrodynamic aspects.

In this section, it has been demonstrated that the transients from 2C geometries exhibit two typical events associated with drying of the front end and the rear cone, which determine the transit time of the interface along the sensor head. A close link between the probe geometry and its latency length is now ensured. However, the cleaved tips produce pre-signals which can induce strong erroneous phase detections. One possibility could be the systematic exploitation of this phenomena as the signature of normal impacts, so that it can be used as an angle discriminator. As for 1C probes, experiments show that pre-signals fluctuate greatly in a two-phase flow because of variations of the impact angle, and an automatic detection may be quite

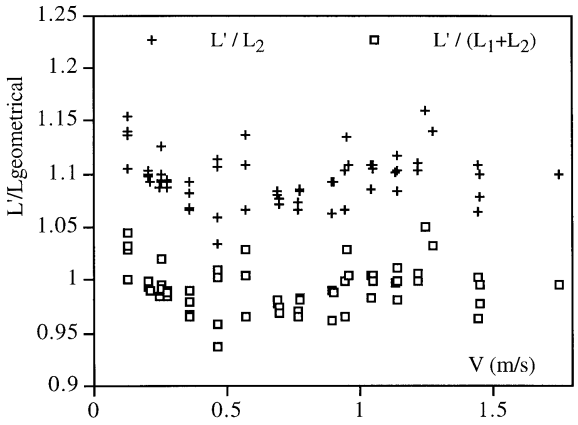


Fig. 12. Latency length evolution for probe 2C05.

Table 1
Some characteristics of manufactured 3C probes

| Probe number | L1 $\mu$m | L2 $\mu$m | L3 $\mu$m | D1 $\mu$m | Total length $L_T$ mm |
|---|---|---|---|---|---|
| 3C06 | 104 | 1362 | 125 | 65 | 1.6 |
| 3C12 | 172 | 952 | 95 | 53 | 1.22 |
| 3C14 | 162 | 1031 | 85 | 44 | 1.28—photo 2b |
| 3C15 | — | — | 88 | — | $L1 + L2 = 1.2$ mm |
| 3C31 | 163 | 525 | 93 | 56 | 0.78 |
| 3C02 | 160 | 320 | 70 | 28 | 0.55 |

difficult to achieve. Again, it is preferable to avoid proximity detection. For this reason, probes ended by a cone instead of a cleaved portion have been designed. This geometry is also very favourable for the reduction of hydrodynamic perturbations.

## 3. Cone + cylinder + cone probes (3C)

No simulation has been attempted for this geometry since by combining the results obtained for 1C (part I) and 2C probes above, the main features of the response of a 3C probe can be imagined. Indeed, the trends identified for 2C probes are expected to remain valid. The main difference is that the fraction of light entering the cylindrical portion is now subject to the cone response instead of that of a cleaved fiber. Accordingly, the plateau level should be modified. This geometry has been directly investigated with experiments using prototypes like that presented in Fig. 2b. To precisely check the capabilities of 3C probes, the length $L_2$ has been first chosen quite large, above 1 mm. In order to detect smaller bubbles, lengths about 300 $\mu$m have been also manufactured, as shown in Table 1. Half-cone angles are still close to 14°. By examining the photographs of Fig. 2b, it appears that the front cone is well formed, while a defect is again present at the base of the rear cone, confirming that this manufacturing defect is due to the influence of the cladding on the etching process.

Quasi-steady piercing experiments have been performed for probe 3C06 whose total length $L_T$ from tip to the base of the cone is about 1.6 mm. The transition observed during water exit

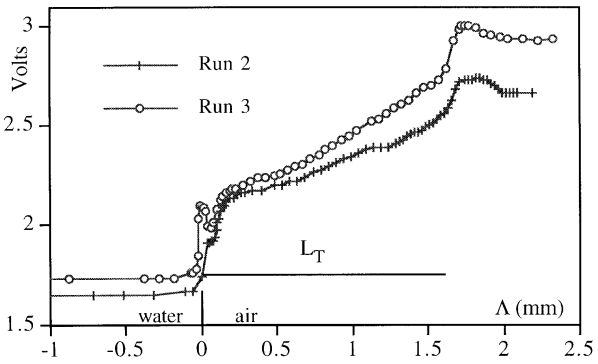


Fig. 13. Quasi-steady water exit response for probe 3C06.

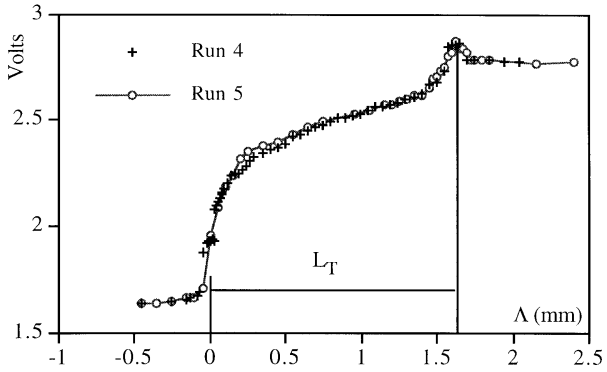


Fig. 14. Quasi-steady inversed water exit response for probe 3C06.

at normal incidence, shown in Fig. 13, is in agreement with the expected response. Indeed, a first steep surge takes place when the probe tip hits the interface, and afterwards the signal increases smoothly over a distance comparable to that of the cylinder $L_2$. A final surge leads to the gas level after a weakly marked maximum. This contribution from the base cone is weak, as expected for this large cylinder diameter (65 $\mu$m). For the two runs, it seems that a small amount of proximity detection is present within $\pm 50\,\mu$m from the undisturbed interface position $\Lambda = 0$. This is compatible with the functioning of conical probes, since it has been shown that a small tip defect can provide a pre-signal. As for conical probes, the peaks near $\Lambda = 1.8$ mm in Fig. 13 are related to the geometrical imperfection located at the base of the rear cone. The more important difference from the expected transient is the steady increase of the signal instead of a constant plateau when the interface travels along the cylindrical portion of the probe. Such an evolution can be possibly induced by surface contamination such as solids particles sticking on the fiber (no special care was taken during these tests), or may be due to some meniscus influence.

A complementary experiment has been performed for an inverted water entry condition, i.e. for a probe with its tip, initially dry and pointing upwards, and which is progressively wetted when moved downward. The signal evolution, given in Fig. 14, is similar to the water exit

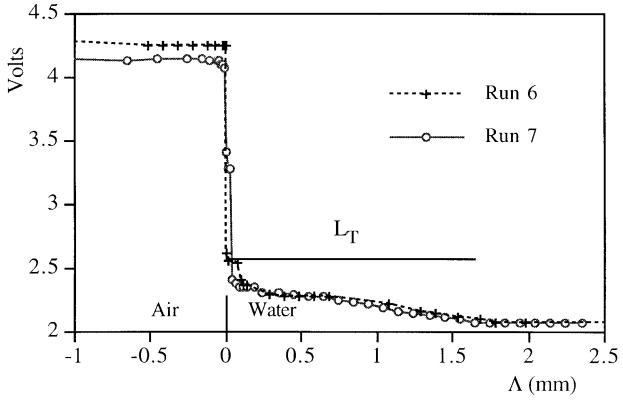


Fig. 15. Quasi-steady water entry response for probe 3C06.

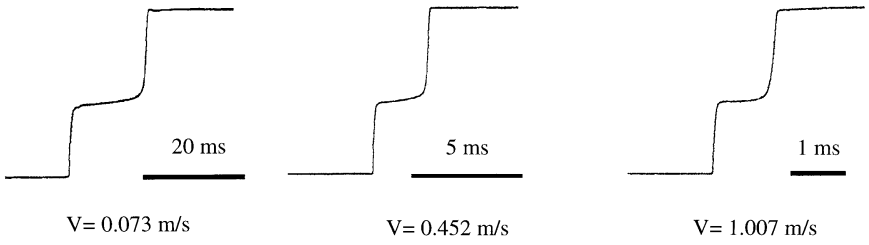


Fig. 16. Water entry transitions for probe 3C15 (the time increases from left to right).

configuration. However, the amplitude of the plateau is higher, while according to our idealised model it should be the same. The reasons for such behaviour are not clear. Note also that proximity detection is not seen here because, due to the inverted meniscus formed during a reversed water entry, the distance between tip and interface is too large (more than 1 mm) when the undisturbed interface reforms. Again, the transition is achieved within a distance almost equal to the total tip length.

During water entry, probe 3C06 provides the transient of Fig. 15. The signal abruptly decreases almost 50% from the gas level, then a slow decrease down to the liquid level occurs within a distance comparable to that of the sensor. Here, the prediction of the optical model is again confirmed: the front cone ensures the first decrease which is strong due to the high coupling in the cylinder (both because $D_1$ is large and because the base cone is in air), the loss for the cylindrical portion is very weak, and the remaining signal drop is seen once the rear cone is covered by water. This response takes place over a distance comparable to the total length.

Qualitatively, 3C probes react in the expected way for quasi-static conditions. The main difference with the simulation concerns the plateau associated with the cylindrical portion: the signal increases with $\Lambda$ instead of being constant for this particular probe.

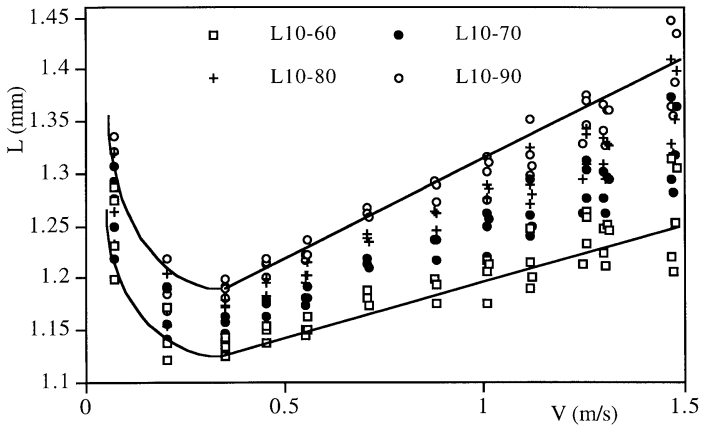


Fig. 17. Latency length of probe 3C15 for various upper thresholds.

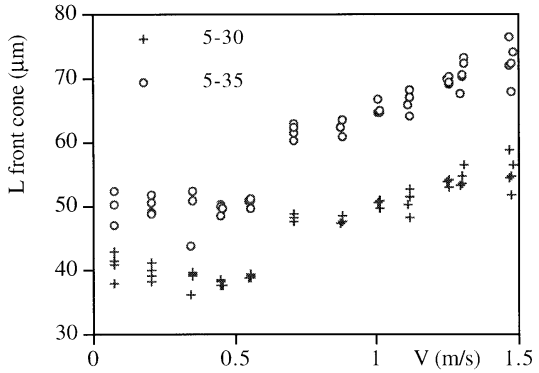


Fig. 18. Contribution of the front cone to the latency length of probe 3C15.

Controlled piercing tests have been performed with various 3C probes interacting with isolated slugs at a normal incidence. Examples of signals corresponding to water entries are given in Fig. 16 and again, step-type shapes are obtained. Compared with 2C probes, pre-signals are absent, as expected. The remarkable feature is that, for moving interfaces, the plateau is now fairly constant and its level does not change much with velocity. It is, however, not ascertained that such a behaviour is due to the moving interface, since different probes have been used for quasi-static and dynamics tests. For probe 3C15, the plateau level stays equal to 44%, while for probe 3C14, it is about 50% for 0.07 m/s and 60% for 1.4 m/s. These levels still depart from the predicted value of 36% using a 2C geometry. Also, the transients during gas entry across a moving interface are similar to the response of Fig. 14 obtained under quasi-static conditions.

The latency length of probe 3C15 is plotted for various upper thresholds in Fig. 17. The magnitude of $L$ is close to the total probe length of about 1.2 mm. All curves have similar trends: the continuous decrease of $L$ with the upper threshold level indicates that some portion

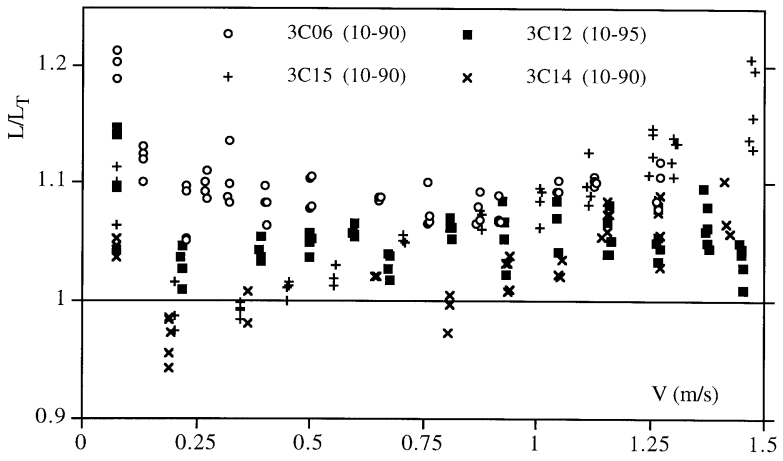


Fig. 19. Comparison between latency lengths of 3C probes made dimensionless by the total tip length $L_T$.

of the rear cone response is progressively missed. The influence of the lower threshold can be appreciated by considering the duration of the first surge corresponding to the response of the front cone. From Fig. 18, it can be estimated to be less than 80 $\mu$m, a value in agreement with the geometrical length $L_3$. In both figures, $L$ increases almost linearly with the velocity above its critical value. From Figs. 17 and 18, it is clear that the front and rear cones are responsible for the lengthening of the transitions and such behaviour has already been observed for conical probe 1C09 (see Fig 27, part I).

To check the reproducibility, various 3C probes have been manufactured and tested. Their latency lengths are scaled by the total length of their sensing tip in Fig. 19. All $L/L_T$ ratios are close to unity within the interval of deviation $-8$ to $+22\%$. Probes 3C14 and 3C15 have latency lengths neatly increasing with velocity. For 3C06 and 3C12, $L$ remains almost stable above the critical velocity. These differences are linked to variations in the cone response as discussed in part I. In almost all cases, $L$ is slightly higher (from a few percent up to 10%) than the geometrical total length. Since proximity detection is absent or undetected, and since the measurement uncertainties alone cannot explain these differences, this behaviour is certainly due to the process of dewetting, which lasts longer than the transit time. The arguments evoked for conical probes about the retarding effect of a liquid film on the formation of the signal are expected to remain valid for 3C geometries.

However, the variations of the latency length observed from probe to probe are less important for 3C probes than for conical probes, indicating that a control of $L$ can be ensured during the manufacturing process. It is thus possible, given a velocity range and the available resolution on $T_u$ measurements, to define an optimal length and to manufacture a dedicated probe. Since the latency length is always close to the geometrical length, the velocity magnitude is available within about 20% without performing any calibration. This uncertainty drops to 5% when using a calibration. Such tests would also provide the plateau level so that the thresholding could be adjusted without any risk of error. Thus, 3C geometries offer important advantages for the simultaneous measurement of the gas phase indicator function and gas velocity.

In the previous sections, emphasis has been put on the connection between the probe geometry and the shape of transients under normal piercing conditions. In order to transpose these results to actual two-phase flows, it is necessary to investigate the influence of additional parameters which could vary greatly. This is the purpose of the complementary tests presented in the next section.

## 4. Influence of uncontrollable parameters

Uncontrollable parameters in a probe–gas inclusion interaction for general two-phase flows include the local interface curvature a, the angle $\gamma$ between the probe axis and the angle of impact on the interface $\beta$ (See Fig. 2, part I). Let us analyse these aspects in order to detect the phenomena which could invalidate the use of the $T_u(V)$ correlations established.

### 4.1. Radius of curvature and minimum detectable bubble size

The influence of the local interface curvature a has been shown to be negligible for stretched probes when it exceeds about 30 times the latency length. With 3C probes, $a/L$ ratios about 4–5 have been tested, and no significant effect was noticed. It would be worthwhile analysing the case of lower $a/L$ ratio. Notably, for a ratio approaching unity, additional problems will occur due to incomplete transitions (the sensor tip will be wetted again before becoming entirely dry).

Similar difficulties are encountered for the determination of the minimum bubble size which can be detected by a probe. Roughly, the $L(V)$ plot provides the boundary for a complete and accurate detection of a gas inclusion. Indeed, for an inclusion whose characteristics of size $R$ and velocity $V_0$ correspond to a point located above the $L(V)$ curve, the probe sensing tip is correctly dried and the signal spends some time at the gas level. As a consequence, front and rear interfaces are clearly defined and the signal can be processed accurately. When the characteristics $(R,V_0)$ are located below the $L(V)$ curve, the situation is more confused. Usually, one gets a signal of weaker amplitude and rather smooth (see Fig. 10 in Cartellier, 1992). Its beginning corresponds to the front interface, but the end of the bubble is more difficult to define, and an erroneous gas dwell time could be measured. Such signal distortions are expected to be larger at high incidence $\beta$, a case corresponding to the detection of small chords pierced across large bubbles. In any case, there is a limit under which the signal does not exceed the noise: such bubbles or chords are clearly missed by the processing. Additional studies are necessary to accurately define the minimum detectable chords.

### 4.2. Impact angle $\beta$

It has been observed that the angle of impact $\beta$ strongly alters the correlation $T_u(V)$ for stretched probes: typically, a change of $\beta$ from 0° to 30° produces a 100% increase of the rise time (Cartellier, 1992). For the same variation in $\beta$, the rise time of conical probes increases by 45% (see Table 4, part I—note that for these tests, the angles $\beta$ and $\gamma$ were equal).

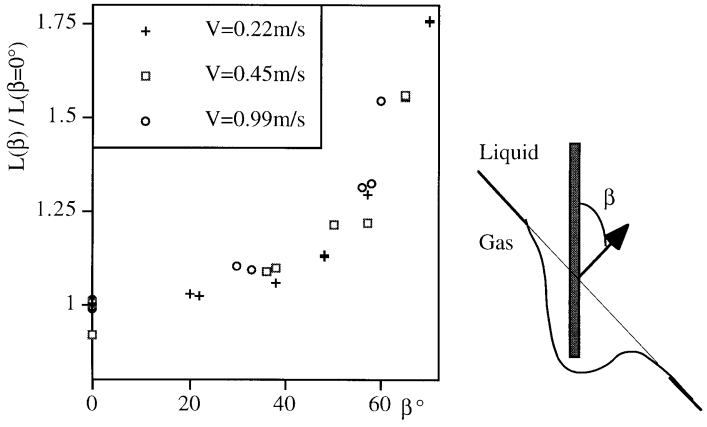


Fig. 20. Influence of the incidence angle $\beta$ on latency length ($\gamma = 0°$, probe 3C15).

Investigations of the influence of $\beta$ have also been performed on probe 3C15. By impacting the nose of slugs at various distances from their axis, $\gamma$ remains equal to zero while $\beta$ is changed. Fig. 20 provides the evolution of $L(\beta)/L(\beta = 0°)$ for three slug velocities $V_0$. Clearly, the transient duration is weakly sensitive to $\beta$. The deviation from the value $L(\beta = 0°)$ corresponding to a normal impact is less than 10% up to $\beta = 40°$. Above this angle, the deviation increases more and more with $\beta$. This behaviour holds whatever the thresholds considered. Since there are no geometrical reasons for an increase in transient durations during oblique impacts, this trend is linked with the liquid film dynamics: the junction of the disturbed interface with its undisturbed position imposes the formation of a liquid finger whose thickness increases with the interface inclination as sketched in Fig. 20.

The weak sensitivity to $\beta$ observed for 3C probes compared to the strong variations previously identified on stretched probes and on conical probes is probably related to the magnitude of the latency length. $L$ is more than 1 mm for the 3C probe used here, and it was about 50 $\mu$m for the stretched tip and the conical probe. Short latency lengths are also expected to be more sensitive to local interface deformations than large ones. It would be worthwhile to measure the evolution of this sensitivity with $L$: this question is left open.

Even with this weaker sensitivity, errors in velocity measurements due to impact angles could be important when using 3C probes. Indeed, the velocity deduced from a signal collected at $\beta = 65°$ is almost twice the actual value! Some means to circumvent this difficulty will be discussed in Section 4.

### 4.3. Velocity orientation angle $\gamma$

Nothing was known about the influence of the angle $\gamma$ characterising the inclination of the bubble velocity to the probe axis. Thus, this effect has been investigated for 3C probes using the experimental facility presented in part I. Under these conditions, the angles $\gamma$ and $\beta$ are identical when hitting the bubble nose. For probe 3C31, the evolution of $L(\gamma = \beta)/L(\gamma = \beta = 0°)$ given in Fig. 21 demonstrates that the transient duration decreases as $\gamma$ increases. This effect cannot be attributed to the incidence $\beta$ since $\beta$ alone has an opposite

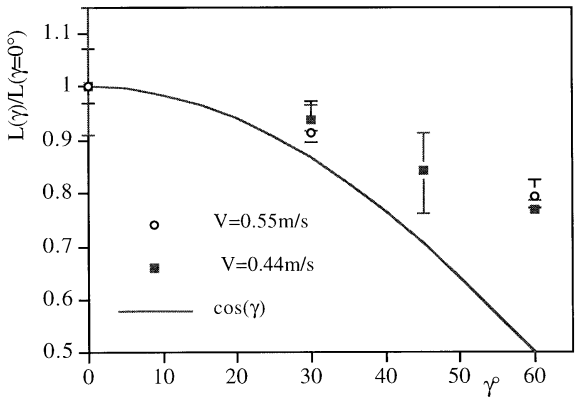


Fig. 21. Influence of the angle $\gamma$ on latency length ($\beta = \gamma$, probe 3C31).

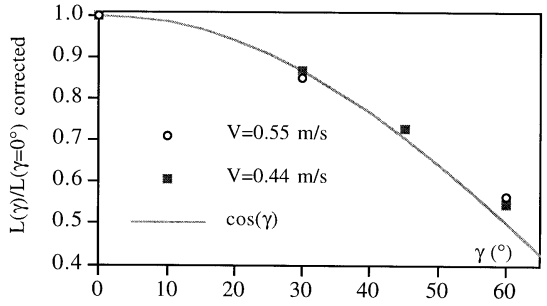


Fig. 22. Latency length corrected from the influence of $\beta$ (probe 3C31).

effect on $L$. Thus, the observed trend is due to the angle $\gamma$ between the probe support and the velocity of the bubble. The reduction of the transit time reaches 20% as $\gamma$ approaches 60%. One can think in terms of geometry to explain this trend. Indeed, neglecting the interface curvature (which is about few centimetres at the nose of bubbles, to be compared to the probe sensing length which is about 0.7 mm), the ideal transit time is defined as the projected probe length $L_T \cos(\gamma)$ divided by the bubble velocity $V_0$. Thus, $L(\gamma)/L(0^\circ)$ should be similar to $\cos(\gamma)$. The comparison shown in Fig. 21 demonstrates that it is not exactly so; the transients are still longer than expected from purely geometrical considerations. However, such a discrepancy could be induced by the angle $\beta$ which was always equal to $\gamma$ in these experiments. In order to isolate the influence of $\gamma$, it has been assumed that the angles $\gamma$ and $\beta$ have a cumulative effect on the latency length. Hence, using the results of Fig. 20, the latency length $L(\gamma, \beta = 0^\circ)$ has been estimated as $L(\gamma, \beta = \gamma)$ divided by $L(\gamma = 0, \beta)$. As shown in Fig. 22, with such a correction, the latency length fits very well the $\cos(\gamma)$ law. Although complementary tests for $\beta = 0^\circ$ and for larger inclinations $\gamma$ should be welcome to confirm these findings, it can be concluded that monofiber optical probes are sensitive to the projection of the velocity along their axis. With these sensitivity analyses in hand, it is now possible to discuss the practical value of the monofiber technique for velocity measurement and for phase detection.

## 5. Discussion of the monofiber technique

### *5.1. Nature of the velocity detected*

To ensure a clear connection with modelling, it is important to define the nature of the gas velocity measurable with monofiber probes. All calibrations have been performed either on the nose of isolated slugs, or on the front part of ellipsoidal bubbles. Provided that normal impacts are considered ($\gamma = \beta = 0^\circ$), this is equivalent to the interpretation of the $L(V)$ curves with velocity equal to the interface displacement velocity. However, the experiments performed for finite inclinations $\beta$ in Section 3C have demonstrated that the interface displacement velocity is not the correct reference. On the contrary, the influence of the angle between the velocity and the probe axis is taken into account by considering the projection of the centre of mass velocity $V_0$. Thus, it is legitimate to interpret the calibration curves as giving access to the projection of the mass centre velocity $V_0$ along the fiber axis. Such a variable is convenient for

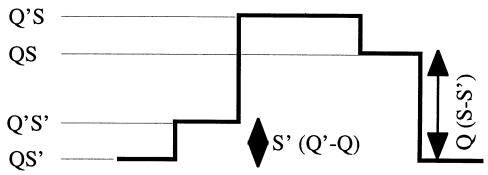


Fig. 23. Schematic transitions for a gas inclusion travelling toward the tip of a 3C probe.

two-phase models. Also, the local gas fluxes are accessible by weighting these velocities by the corresponding gas presence time: this provides a simple means of checking the performance of the monofiber probes.

The above considerations have been proven valid for $\gamma$ within the limits $\pm 60^\circ$, so that a wide range of two-phase flows can be analysed with the monofiber technique. Its extension to more complex flow fields requires additional studies for large angles $\gamma$. Beside, it should be very interesting to be able to determine the direction of the gas velocity, notably in order to detect secondary flows. Such detection may be envisaged using 3C probes. Indeed, according to the schematic functioning presented in Section 1A, a gas inclusion travelling along the probe from its base up to its tip is expected to deliver the signature presented in Fig. 23. Compared with the signature obtained for a positive velocity, i.e. for an inclusion travelling from the tip to the base (see Fig. 8), there is a strong difference in the amplitude of the intermediate plateau of the ascending ramp: its level is lower for a negative velocity than for a positive one. Since this behaviour has been indeed observed during controlled piercing experiments for probe 3C02, the amplitude of the intermediate plateau can be an indicator of the flow direction. However, the feasibility of this proposal remains to be checked for a probe immersed in two-phase flow. Beside, one should notice that such inverted signatures are expected to appear mainly for inclusions much larger than the probe because of the wetting characteristics of the liquid, and the above sign detection is probably not possible for finely dispersed suspensions.

### 5.2. Selection of meaningful transitions

A crucial difficulty remains since it is unavoidable that the uncontrollable variable $\beta$ appears as a parameter in the general $T_u(V_0)$ correlation. For 3C probes, and for $\beta$ in the range $\pm 40^\circ$, the dispersion on velocities due to $\beta$ is limited to 10%, but outside this range, the error increases drastically up to more than 70%. To ensure accurate velocity measurements, it is thus necessary to apply the correlation only for meaningful transitions. However, owing to the variability of bubbles shapes and positions in a gas–liquid flow, almost all values of the incidence $\beta$ can interact with the probe, and this objective seems unattainable without any discrimination on this angle. The experience seems to contradict this expectation since Pinguet (1994) has reported velocity uncertainties in the range $\pm 25\%$, apparently without using any discrimination.

It is nevertheless recommended to introduce some validation criteria to select meaningful transitions. A first aspect is that the probe dewetting must be completed: this can be checked by the presence of a plateau at the gas level. Regarding discrimination on the angle $\beta$, there is not yet any general rule. However, an efficient criterion based on a time ratio, proposed by

Cartellier (1992), has led to a velocity uncertainty of about 13% in bubbly flow even using a monofiber stretched probe which was not optimised for velocity measurements. This proposal is valid for small gas inclusions, say about few millimetres in size, but it is probably poorly efficient for Taylor bubbles or distorted slugs. Also, additional problems may occur for wobbling interfaces, especially if $L$ becomes comparable to the local interface curvature.

Let us mention that another possibility to ensure a discrimination on $\beta$ would be to use multiple probes with an appropriate logic in order to determine the bubble position relative to the probe: such devices have been studied by some authors (Burgess and Calderbank, 1975; Revankar and Ishii, 1993). In the same prospect, the combination of multiple probes with multiple rise time measurements may provide a practical solution to get access to many velocity components and then to the mean interfacial area using the model of Kataoka et al. (1986).

### *5.3. Additional comments concerning the signal processing*

Let us briefly discuss some of the requirements which must be fulfilled by the signal processing in order to extract the gas indicator functions and gas velocities. For phase detection, any time proximity detection is avoided or minimised, both 1C and 3C geometries provide an accurate indication of the start and the end of bubbles, provided that the gas chord exceeds the sensor latency length. When this is not the case, the signals become distorted and the precise definition of the end of such signatures in connection with the position of the interface is an open question. In any case, the start of a bubble cannot be identified within the noise level affecting the signal, so there is a clear advantage in ensuring the best SNR on raw signals.

For rise time measurements, the threshold levels are to be set according to the calibration of the latency length $L$. It is also necessary to accurately determine the water and air levels. Practice shows that the water level is usually very stable (unless strong fouling is present), so that it needs to be determined only once. In contrast, the gas level should be estimated for each event detected by the probe. As mentioned above, the correlation applies only if the entire probe tip is engulfed in the gas phase: signal processing must be able to identify such events. Then the transitions should be selected to reduce the range of impact angles $\beta$. Once the rise times are available for a sub-set of events, they have to be translated into velocities. For that, instead of the ideal transit time law, i.e. $V_0 = L^*/T_u$, it is recommended to use directly the correlation in the form $T_u(V_0)$ because it integrates all departures from the ideal law. Indeed, such a form is able to account for the region of low velocities, and for any specific response such as those leading to an increase of $L$ with $V_0$. The typical dispersion of these calibrations due to incomplete experimental control of the piercing conditions is about $\pm 5\%$: such an uncertainty is less than the dispersion induced by the variations of impact conditions in two-phase flow.

Based on the above recommendations, a real time signal processing has been designed. In combination with 1C or 3C probes, it provides the distributions of gas residence times as well as those of rise times. According to preliminary qualifications, and despite the various problems mentioned above, the proposed technique has been proved to be quite efficient in co-current air/water flows (Cartellier et al., 1996). A future article will be devoted to the detailed description of signal processing, and to the analysis of the performance of this new measurement technique.

## 6. Conclusion

A new probe design consisting of a cylinder and a cone has been analysed. It has been shown that its response while crossing water–air interfaces can be interpreted as a double switch, one due to the base cone and the other due to the front cleaved end. The corresponding rise time is then closely connected to the probe geometry so that a precise control of the latency length can be ensured during the manufacturing process. To maintain such an advantage while avoiding pre-signals, prototypes composed of a cone, a cylinder and a cone have been investigated. This geometry has been optimised to ease the detection of signal transitions. It has been shown that such shapes provide the velocity of the gas inclusion projected along their axis. In addition, this geometry is weakly sensitive to the impact angle, as opposed to stretched or conical probes. To improve the accuracy of velocity measurements, a discrimination on the impact angle is nevertheless recommended.

It is worth mentioning that, for the monofiber technique, there is no foreseeable limit in terms of velocity magnitude provided that the rise times remain unaltered by the electronic bandwidth. In practice, $L$ can be adjusted to fit this constraint according to the magnitude of the velocity expected.

The feasibility of the gas velocity measuring principle has been well established for air and water, but it is certainly valid for other combinations of fluids, including liquid/liquid suspensions. However, the duration of the transitions is expected to change notably with liquid viscosity and the ratio of densities which alter the interface deformation, so that a calibration is recommended for any extension of the technique to different fluids.

## Acknowledgements

The authors are grateful to the DER-EdF for support of this research under grant no. EdF T34L01/2K6727/RNE402. They are also thankful to P. Benech, LEMO, Grenoble for insightful discussions about probe manufacture and optical modelling.

## References

Bobb, L., Krumboltz, H., Davis, J. 1988. An optical fiber refractometer. Proceedings of SPIE. Chemical, Biochemical and Environmental Applications of Fibers. 990. pp. 164–169.

Burgess, J., Calderbank, P., 1975. The measurement of bubble parameters in two-phase dispersions—I. The development of an improved probe technique. Chemical Engineering Science 30, 743–750.

Cartellier, A., 1992. Simultaneous void fraction measurement, bubble velocity, and size estimate using a single optical probe in gas–liquid two-phase flows. Review of Scientific Instruments 63 (11), 5442–5453.

Cartellier, A., Barrau, E., Poupot, Ch, Chambérod, E., 1996. Sondes optiques: innovations sur un capteur classique. La Houille Blanche 1/2, 120–128.

Cartellier, A., Barrau, E., 1998. Monofiber optical probes for gas detection and gas velocity measurements: conical probes (referred to as part I). International Journal of Multiphase Flows 24, 1265–1294.

Kataoka, I., Ishii, M., Serizawa, A., 1986. Local formulation and measurements of interfacial area concentration in two-phase flow. International Journal of Multiphase Flows 12 (4), 505–529.

Pinguet, B., 1994. Étude de sondes d'impédance pour la caractérisation d'écoulements diphasiques liquide-liquide en conduite inclinée. Doctorat de l'Univ, Pierre et Marie Curie, 16 Déc, Paris.